Научном већу Института за физику у Београду

Предмет: Молба за покретање поступка за стицање звања истраживач сарадник

Пошто испуњавам све предвиђене услове у складу са Правилником о стицању истраживачких и научних звања МПНТР, молим Научно веће Института за физику у Београду да покрене поступак за мој избор у звање истраживач сарадник.
У прилогу достављам:

1 мишљење руководиоца лабораторије са предлогом чланова комисије за избор у звање;
2 стручну биографију;
3 преглед научне активности;
4 списак објављених научних радова;
5 уверење о уписаној години докторских студија;
6 копију диплома основних и мастер академских студија;
7 уверење о прихваћеној теми докторске дисертације;
8 копије објављених радова.

Са поштовањем,
Сузана Миладић
истраживач приправник
Сузи Мила

УНИВЕРЗИТЕТ У БЕОГРАДУ
ИНСТИТУТ ЗА ФИЗИКУ | БЕОГРАД
ИНСТИТУТ ОД НАЦИОНАЛНОГ ЗНАЧАЈА ЗА РЕПУБЛИКУ СРБИЈУ
www.ipb.ac.rs

Број 0801-1267/2

Датум 30. 09. 2022

Научном већу Института за физику у Београду

Београд, 28. септембар 2022. године

Предмет: **Мишљење руководиоца лабораторије о избору Сузане Миладић у звање истраживач сарадник**

Сузана Миладић је запослена у Лабораторији за примену рачунара у науци, у оквиру Националног центра изузетних вредности за изучавање комплексних система Института за физику у Београду. Под руководством др Ненада Вукмировића ради на докторској дисертацији из електронских особина полупроводника. С обзиром да испуњава све предвиђене услове у складу са Законом о науци и истраживањима и Правилником о стицању истраживачких и научних звања МПНТР, сагласан сам са покретањем поступка за избор Сузане Миладић у звање истраживач сарадник.

За састав комисије за избор Сузане Миладић у звање истраживач сарадник предлажем:

(1) др Ненад Вукмировић, научни саветник, Институт за физику у Београду
(2) др Дарко Танасковић, научни саветник, Институт за физику у Београду
(3) др Божидар Николић, ванредни професор Физичког факултета Универзитета у Београду
(4) др Антун Балаж, научни саветник, Институт за физику у Београду

др Антун Балаж
научни саветник
Руководилац Лабораторије за примену рачунара у науци

Биографија Сузане Миладић

Сузана Миладић је рођена 1995. године у Новом Саду. Завршила је основну школу „Десанка Максимовић” у Бачкој Паланци 2010. године као ђак генерације. Потом уписује средњу медицинску школу „7. април” у Новом Саду на смеру Физиотерапеутски техничар и исту завршава 2014. године као добитник Вукове дипломе.

Школовање наставља на Природно-математичком факултету Универзитета у Новом Саду где дипломира 2018. године на смеру Физичар-истраживач са просечном оценом 9,55. Студије физике наставља на Физичком факултету Универзитета у Београду уписавши мастер студије на смеру Теоријска и експериментална физика. Мастер студије завршава у септембру 2019. године одбраном рада „Спинска резонанца и релаксација у квантним тачкама унутар InSb наножица” који је радила под менторством Марка Миливојевића и др Едиба Добарџића, који је био и руководилац рада. Мастер рад је награђен наградом Физичког Факултета “Проф. Др Љубомир Ћирковић”. Мастер студије завршава са просечном оценом 9,67.

Докторске студије уписује 2019. године на Физичком факултету Универзитета у Београду на смеру Физика кондензоване материје и статистичка физика. Запослена је на Институту за физику у Београду као истраживач приправник у Лабораторији за примену рачунара у науци, у оквиру Националног центра изузетних вредности за изучавање комплексних система. Истраживање везано за докторски рад врши под менторством др Ненада Вукмировића на темама везаним за електронски транспорт у полупроводницима.

Преглед научне активности кандидата

У оквиру научног рада везаног за докторат, кандидат Сузана Миладић се бави истраживањем транспорта у системима са електрон-фонон интеракцијом. Конкретно, у досадашњем раду предмет истраживања кандидата био је транспорт поларона једнодимензионог Холштајновог модела.

Поларонски транспорт се сматра једним од доминантних механизама провођења у органским полупроводницима који данас налазе широку техничку примену. Холштајнов модел, који до данас није у потпуности решен, представља један од најједноставнијих модела за систем са електрон-фонон интеракцијом. Успешно решење транспорта Холштајновог поларона нас води ближе ка истраживању транспорта у реалним материјалима.

Динамичка својства Холштајновог модела су испитана за екстремне случајеве, као што су лимити јаке или слабе електрон-фонон интеракције где су примењиве апроксимативне методе. Истраживачки рад кандидата је фокусиран на истраживање транспорта Холштајновог поларона у широком опсегу параметара користећи се нумерички егзактним методама без увођења апроксимација на хамилтонијан.

Већ устаљени приступ за егзактно третирање система у физици је Path Integral Monte Carlo (PIMC) метод. Покретљивост поларона се према Кубовој формули може добити уколико је позната струја-струја корелациона функција. PIMC метод се састоји из тога да се дефинише Path Integral репрезентација за тражену корелациону функцију, а потом се суме и интеграли који се у том изразу јављају решавају нумерички применом Monte Carlo техника. Постоје значајна ограничења која се јављају при оваквом приступу. Највећа потешкоћа јесте динамички проблем знака који се испољава при одређивању временских корелационих функција Monte Carlo техникама. Стандардни приступ којим се овај проблем заобилази је одређивање временске корелационе функције на имагинарној оси те аналитичко продужење добијених података на реалну осу. Међутим, само аналитичко продужење дискретних података је велики проблем само за себе.

У досадашњем раду кандидат је успешно развио метод за одређивање струја-струја корелационе функције на основу PIMC метода при чему је значајно умањен утицај динамичког проблема знака. Такође, у сарадњи са ментором, развијен је метод за добијање покретљивости путем аналитичког продужења користећи податке за струја-струја корелациону функцију са реалне и са имагинарне осе.

Користећи развијене технике за одређивање струја-струја корелационе функције даље истраживање кандидата иде у смеру одређивања покретљивости Холштајновог поларона за широк опсег параметара хамилтонијана. На овај начин могуће је одредити транспортне режиме поларона те испитати могуће приближне методе (јефтиније и нумерички ефикасније) које би се у тим режимима могле успешно применити. То нам отвара пут ка даљем истраживању које би било фокусирано на транспорт сложенијих модела са електрон-фонон интеракцијом и у крајњем и реалних материјала.

Списак научних радова кандидата

Категорија М21

[1] **S. Miladić**, P. Stipsić, E. Dobardžić, and M. Milivojević, *Electrical control of a spin qubit in InSb nanowire quantum dots: Strongly suppressed spin relaxation in high magnetic field,* Phys. Rev. B **101**, 155307 (2020)

Категорија М34

[1] **S. Miladić,** N. Vukmirovic, *Mobility of Holstein polaron from real and imaginary time quantum Monte Carlo calculations,* BPU11 CONGRESS, 28 August 2022 – 1 September 2022, Book of abstracts P:126

Република Србија
Универзитет у Београду
Физички факултет
Д.Бр.2019/8010
Датум: 21.09.2022. године

На основу члана 161 Закона о општем управном поступку и службене евиденције издаје се

УВЕРЕЊЕ

Миладић (Синиша) Сузана, бр. индекса 2019/8010, рођена 03.01.1995. године, Нови Сад, Република Србија, уписана школске 2021/2022. године, у статусу: финансирање из буџета; тип студија: докторске академске студије; студијски програм: Физика.

Према Статуту факултета студије трају (број година): три.
Рок за завршетак студија: у двоструком трајању студија.

Ово се уверење може употребити за регулисање војне обавезе, издавање визе, права на дечији додатак, породичне пензије, инвалидског додатка, добијања здравствене књижице, легитимације за повлашћену вожњу и стипендије.

Овлашћено лице факултета

Република Србија
Универзитет у Београду
Физички факултет
Д.Бр.2019/8010
Датум: 21.09.2022. године

На основу члана 161 Закона о општем управном поступку и службене евиденције издаје се

УВЕРЕЊЕ

Миладић (Синиша) Сузана, бр. индекса 2019/8010, рођена 03.01.1995. године, Нови Сад, Република Србија, уписана школске 2021/2022. године, у статусу: финансирање из буџета; тип студија: докторске академске студије; студијски програм: Физика.

Према Статуту факултета студије трају (број година): три.
Рок за завршетак студија: у двоструком трајању студија.

Ово се уверење може употребити за регулисање војне обавезе, издавање визе, права на дечији додатак, породичне пензије, инвалидског додатка, добијања здравствене књижице, легитимације за повлашћену вожњу и стипендије.

Овлашћено лице факултета

РЕПУБЛИКА СРБИЈА

УНИВЕРЗИТЕТ У НОВОМ САДУ
ПРИРОДНО-МАТЕМАТИЧКИ ФАКУЛТЕТ,
НОВИ САД

Оснивач: Република Србија
Аутономна Покрајина Војводина
Дозволу за рад 114-022-423/2012-01 од 18. 09. 2012. године је издала
Аутономна Покрајина Војводина, Покрајински секретаријат за науку и технолошки развој

ДИПЛОМА

Сузана (Синиша) Миладић

рођена 03. 01. 1995. године у Новом Саду, општина Нови Сад, Република Србија, уписана школске 2014/2015. године, а дана 28. 09. 2018. године завршила је основне академске студије првог степена на студијском програму ФИЗИКА обима 240 (две стотине четрдесет) бодова ЕСПБ са просечном оценом 9,55 (девет и 55/100).

На основу тога издаје се ова диплома о стеченом високом образовању и стручном називу

ДИПЛОМИРАНИ ФИЗИЧАР

Број дипломе: 3883-324/14, 12. 12. 2018. године
У Новом Саду

ДЕКАН
Проф. др Милица Павков Хрвојевић

РЕКТОР
Проф. др Дејан Јакшић

UNS08BH06858

Универзитет у Београду
Физички факултет
Број индекса: 2018/7029
Број: 2302019
Датум: 25.09.2019.

На основу члана 161 Закона о општем управном поступку ("Службени лист СРЈ", бр. 33/97, 31/2001 и "Службени гласник РС", бр. 30/2010) и службене евиденције, Универзитет у Београду - Физички факултет, издаје

У В Е Р Е Њ Е

Сузана Миладић

име једног родитеља Синиша, ЈМБГ 0301995805057, рођена 03.01.1995. године, Нови Сад, Република Србија, уписана школске 2018/19. године, дана 23.09.2019. године завршила је мастер академске студије на студијском програму Теоријска и експериментална физика, у трајању од једне године, обима 60 (шездесет) ЕСПБ бодова, са просечном оценом 9,67 (девет и 67/100).

На основу наведеног издаје јој се ово уверење о стеченом високом образовању и академском називу **мастер физичар.**

Декан

Проф. др Иван Белча

ДОКТОРСКЕ СТУДИЈЕ

ПРЕДЛОГ ТЕМЕ ДОКТОРСКЕ ДИСЕРТАЦИЈЕ КОЛЕГИЈУМУ ДОКТОРСКИХ СТУДИЈА

Школска година 2021/2022

Подаци о студенту

Име: Сузана

Презиме: Миладић

Број индекса: 3010/2019

Научна област дисертације: Физика кондензоване материје и статистичка физика

Подаци о ментору докторске дисертације

Име: Ненад

Презиме: Вукмировић

Научна област: Физика кондензоване материје и статистичка физика

Звање: научни саветник

Институција: Институт за физику у Београду

Предлог теме докторске дисертације

Наслов

Quantum Monte Carlo study of polaron mobility

(Проучавање покретљивости поларона користећи квантне Монте Карло методе)

Уз пријаву теме докторске дисертације Колегијуму докторских студија, потребно је приложити следећа документа:

1. Семинарски рад (дужине до 10 страница)
2. Кратку стручну биографију писану у трећем лицу једнине
3. Фотокопију индекса са докторских студија

Потпис ментора

Датум 19.08.2022.

Потпис студента

Мишљење Колегијума докторских студија

Након образложења теме докторске дисертације Колегијум докторских студија је тему

прихватио ☑
није прихватио ☐

Датум

21.09.2022

Продекан за науку Физичког факултета

Electrical control of a spin qubit in InSb nanowire quantum dots: Strongly suppressed spin relaxation in high magnetic field

Suzana Miladić,[1] Pavle Stipsić,[1] Edib Dobardžić,[1] and Marko Milivojević[2,3]
[1]*Faculty of Physics, University of Belgrade, Studentski trg 12, 11001 Belgrade, Serbia*
[2]*NanoLab, QTP Center, Faculty of Physics, University of Belgrade, Studentski trg 12, 11001 Belgrade, Serbia*
[3]*Department of Theoretical Physics and Astrophysics, Faculty of Science, P. J. Šafárik University, Park Angelinum 9, 040 01 Košice, Slovak Republic*

(Received 20 November 2019; revised manuscript received 2 February 2020; accepted 3 April 2020; published 22 April 2020)

In this paper we investigate the impact of gating potential and magnetic field on phonon induced spin relaxation rate and the speed of the electrically driven single-qubit operations inside the InSb nanowire spin qubit. We show that a strong g factor and high magnetic field strength lead to the prevailing influence of electron-phonon scattering due to deformation potential, considered irrelevant for materials with a weak g factor, like GaAs or Si/SiGe. In this regime we find that spin relaxation between qubit states is significantly suppressed due to the confinement perpendicular to the nanowire axis. We also find that maximization of the number of single-qubit operations that can be performed during the lifetime of the spin qubit requres single quantum dot gating potential.

DOI: 10.1103/PhysRevB.101.155307

I. INTRODUCTION

Spin of an electron confined in a semiconductor quantum dot (QD) can act as a carrier of quantum information [1] and a building block of quantum computers. In order to manipulate electron spin, usage of the external magnetic [2,3] and electric [4–6] field was suggested. Although spin control by means of a magnetic field is straightforward, electrical control of spin qubit through electric-dipole spin resonance (EDSR) is technologically more desirable [7–10].

Spin-orbit coupling (SOC) plays an essential role in the EDSR spin qubit scheme, since it allows transitions between qubit states using the spin-independent driving, such as electric-dipole interaction. On the other hand, the presence of SOC induces undesired phonon mediated transitions between qubit states [11–21]. In order to suppress the coupling to phonons, approaches like the optimal design of QDs [22,23] or the control of system size [24] was suggested.

Relaxation rates are dependent on the full three-dimensional QD potential, but in most cases contribution of the confinement along the direction(s) perpendicular to the substrate in which QDs are embedded can be neglected. Assuming magnetic fields up to several tesla, this reduction is justified in material with a weak effective Landé g factor. A typical example that satisfies this assumption are lateral GaAs QDs [25], while in the opposite direction lies an InSb nanowire, having two orders of magnitude stronger g factor [26]. Having also very strong SOC, spin qubits in InSb nanowires [27–31] have attracted much attention due to the observed [28] fast electric-dipole induced transition between qubit states, whose speed is equal to the strength of Rabi frequency.

Since both Rabi frequency and phonon induced relaxation rates are dependent on the magnetic field orientation and strength, design of the gating potential, and SOC, there is a wide range of possibility to tune their strength, with the goal of obtaining as much as possible single-qubit operations during its lifetime.

In this paper we search for the optimal regime in which electrical control of the InSb spin qubit can be achieved. We analyze both single and double quantum dot (DQD) potential and discuss its positive features and negative drawbacks on the spin qubit. In the case of double quantum dot potential, there is the possibility to tune the distance between the dots and to analyze the effects of the asymmetric gating potential. Also, we address the situations in which full three-dimensional confinement has nontrivial influence on spin relaxation rates. We will show that scattering by deformation potential dominates in this regime. Finally, to offer a quantitative insight into the spin qubit quality, we define a figure of merit as the ratio of Rabi frequency and the overall spin relaxation rate and discuss the obtained results in terms of this measure.

This paper is organized as follows. In Sec. II the single-electron Hamiltonian model of the InSb nanowire is introduced. In Sec. III we start with the definition of Rabi frequency and phonon induced spin relaxation rate between spin qubit states. After that, we independently study their dependence on tunable parameters of the system. Using the obtained results, quality of the spin qubit is discussed with the help of the figure of merit as a quantitative measure. In the end we finish the paper with a short conclusion and the impact of the presented results.

II. NANOWIRE SPIN QUBIT MODEL

We start with the Hamiltonian describing the electron confined in an InSb nanowire [30]

$$H = \frac{p^2}{2m^*} + V(x) + H_{so} + H_z, \tag{1}$$

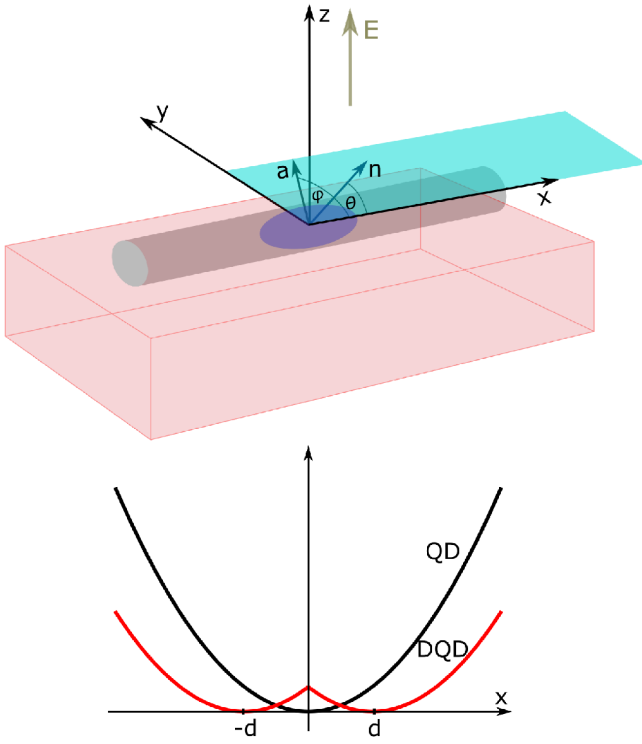

FIG. 1. (Upper panel) *Nanowire QD—schematic view.* Electron dynamics along the nanowire (x) axis is described by the Hamiltonian H, given in Eq. (1). Angle between the nanowire x axis and magnetic field direction $\mathbf{n} = (\cos\theta, \sin\theta, 0)$ is equal to θ, while the spin-orbit vector $\mathbf{a} = (\cos\varphi, \sin\varphi, 0)$ builds an angle φ with the x axis. (Lower panel) Confining potential used in Eq. (1): QD and DQD potential. In the case of a DQD potential [Eq. (6)] symmetric confinement is depicted ($\omega_L = \omega_R$), with distance between the dots equal to $2d$.

where m^* is the effective mass, $p = -i\hbar\partial/\partial_x$ momentum in x direction, $V(x)$ is the gating potential used to localize the electron, while $H_{\rm so}$ represents the spin-orbit interaction Hamiltonian consisting of two terms: Dresselhaus [32] and Rashba [33]. The presence of the Dresselhaus SOC is due to the material in which an electron is embedded. On the other hand, Rashba SOC appears when an electric field E in the z direction is applied (see Fig. 1). In an InSb nanowire, a spin-orbit interaction Hamiltonian is equal to [30]

$$H_{\rm so} = (\alpha_D\sigma_x + \alpha_R\sigma_y)p, \tag{2}$$

where σ_x and σ_y are Pauli matrices, while α_D and α_R are Dresselhaus and Rashba spin-orbit coupling strengths. Suitable change of parameters α_R and α_D with $\alpha = \sqrt{\alpha_D^2 + \alpha_R^2}$ and $\varphi = \arctan(\alpha_R/\alpha_D)$ allows us to write Eq. (2) as

$$H_{\rm so} = \alpha\boldsymbol{a}\cdot\boldsymbol{\sigma}p, \tag{3}$$

using the unit spin-orbit vector $\boldsymbol{a} = (\cos\varphi, \sin\varphi, 0)$ and the vector $\boldsymbol{\sigma}$ made of Pauli matrices. Finally, H_z is the Zeeman term, describing the coupling of spin and magnetic field

$$H_z = \frac{g}{2}\mu_B\boldsymbol{B}\cdot\boldsymbol{\sigma}, \tag{4}$$

where g is the effective Landé factor, μ_B is the Bohr magneton, while $\boldsymbol{B} = B\boldsymbol{n}$ is the applied magnetic field in the plane of the substrate, building an angle θ with the growth x axis of the nanowire (see the upper panel of Fig. 1). In this work a magnetic field is considered to be in-plane to minimize the orbital effects [22,34–36]. In Appendix A we have shown that for B up to 3 T, orbital effects of a magnetic field are small and can be neglected.

Typical gating that confines a single electron in experimental setups [37] can be modeled as a harmonic oscillator quantum dot (QD) [38] or double quantum dot (DQD) [29] potential. Corresponding potentials are equal to (see the lower panel of Fig. 1 as an illustration)

$$V^{\rm QD}(x) = \tfrac{1}{2}m^*\omega^2x^2, \tag{5}$$

$$V^{\rm DQD}(x) = \tfrac{1}{2}m^*\min\{\omega_L^2(x+d)^2, \omega_R^2(x-d)^2\}. \tag{6}$$

In the case of a QD potential, the only degree of freedom is the harmonic potential frequency ω, while in the DQD case frequencies ω_L and ω_R can be tuned, as well as the distance $2d$ between the dots. Since DQD potential allows asymmetric confinement, we introduce asymmetry parameter δ, equal to the ratio of frequencies in the left and right dot, $\delta = \omega_L/\omega_R$. Impact of the DQD confinement will be discussed in terms of δ, $2d$, and $\omega_R = \omega$ (more detailed explanation can be found in Sec. III A).

The Hamiltonian of the electron in different potential types and magnetic field strengths can be solved using the numerical diagonalization [39], although perturbative approaches in the study of spin qubit properties are common [21,27,30]. In this work we follow the numerical approach; the numerical procedure used in obtaining the eigenvalues and eigenvectors of the Hamiltonian given in Eq. (1) is explained in Appendix B. In order to successfully diagonalize the Hamiltonian, orbital $x_0 = \sqrt{\hbar/m^*\omega}$ and spin-orbit $x_{\rm so} = \hbar/m^*\alpha$ lengths are defined. In our calculations we have used $m^* = 0.014\ m_e$ [29], $x_0 = 30$ nm [29], and $x_{\rm so} = 165$ nm [40] parameters for both QD and DQD potentials (recall that $\omega_R = \omega$ in the DQD case), related to the experimental reports on InSb nanowires. On the other hand, we have used g factor in bulk InSb material, $g = -51.3$ [41], being in the range of the experimentally reported values [38,42]. Initial check of the numerical recipe presented in Appendix B were exact analytical results obtained in the special case of the infinite square well [43]. In this case we were able to reproduce the results concerning the angular dependence of the energy splitting between Zeeman sublevels, Rabi frequency, and the relaxation rate.

The nanowire Hamiltonian [Eq. (1)] describes the single-electron dynamics in the x direction only. To ensure the validity of the one-dimensional approximation and to suppress the dynamics in the yz plane, a much stronger yz plane confinement than in the x direction is needed. In this case, a wave function along both directions, y and z, will correspond to the respective ground state. To take into the account the wire geometry of the system, the same confinement length $y_0 = z_0 = 10$ nm in the $y(z)$ direction is assumed. We model the confinement potential as harmonic [39], to which the ground state wave function $\psi(y) = e^{-y^2/2y_0^2}/\sqrt{\sqrt{\pi}y_0}$ corresponds. In the z direction an additional potential eEz ($z > 0$; $z = 0$

corresponds to the position of the substrate) is present due to the applied electric field. Finally, the substrate acts as an infinite potential barrier for the confined electron, forbidding him to propagate in the $z < 0$ region [44]. The ground state $\psi(z)$ of the Hamiltonian in the z direction is found using the same numerical method as for the Hamiltonian in the x direction. Thus, the ground state wave function in the yz plane is equal to $\Psi(y, z) = \psi(y)\psi(z)$.

III. EDSR AND SPIN RELAXATION IN NANOWIRE SPIN QUBIT

In order to achieve electrical control of the nanowire spin qubit, an oscillating electric field in the x direction should be switched on, resulting in the Rabi Hamiltonian $H_R = eE_0 x\cos(\omega_E t)$. When the applied electric field is in resonance with our quantum system, Rabi frequency Ω_{01} is defined as

$$\Omega_{01} = \frac{eE_0}{h}|\langle 0|x|1\rangle|, \tag{7}$$

measuring the speed of the single-qubit rotations. In Eq. (7) states $|0\rangle$ and $|1\rangle$ correspond to the ground and first excited state of the single electron Hamiltonian H, while $e|\langle 0|x|1\rangle|$ is the dipole matrix element. We are particularly interested in the case where qubit states are Zeeman sublevels of the orbital ground state, since in this regime strength of the Rabi frequency can be manipulated by changing the magnetic field orientation [30].

Besides providing the opportunity to electrically control the spin qubit, SOC triggers the undesired phonon induced transition between qubit states, setting up a limit on the qubit lifetime. Rate of spin relaxation can be determined from the Fermi golden rule

$$\Gamma_{01} = \frac{2\pi}{\hbar}\sum_{\nu\mathbf{q}}|M_\nu(\mathbf{q})|^2|\langle\psi_0|e^{i\mathbf{q}\cdot\mathbf{r}}|\psi_1\rangle|^2\delta(\Delta E_{01} - \hbar\omega_{\nu\mathbf{q}}). \tag{8}$$

Transition is triggered by acoustic phonons of energy $\hbar\omega_{\nu\mathbf{q}}$ that correspond to the energy separation between qubit states, $\Delta E_{01} = |E_0 - E_1|$. We assume a linear dispersion relation of acoustic phonons with respect to the intensity of wave vector $\mathbf{q}$, $\omega_{\nu\mathbf{q}} = c_\nu|\mathbf{q}|$, yielding $|\mathbf{q}| = \Delta E_{01}/\hbar c_\nu$.

Next, three different geometric factors $|M_\nu(\mathbf{q})|^2$ entering spin relaxation rates originate from different types of electron-phonon scattering: electron-longitudinal phonon scattering due to the deformation potential [45]

$$|M_{\mathrm{LA-DP}}(\mathbf{q})|^2 = \frac{\hbar D^2}{2\rho c_{\mathrm{LA}}V}|\mathbf{q}|, \tag{9}$$

electron-longitudinal phonon scattering due to the piezoelectric field [45]

$$|M_{\mathrm{LA-PZ}}(\mathbf{q})|^2 = \frac{32\pi^2\hbar(eh_{14})^2}{\epsilon^2\rho c_{\mathrm{LA}}V}\frac{(3q_xq_yq_z)^2}{|\mathbf{q}|^7}, \tag{10}$$

where h_{14} is piezoelectric constant, and electron-transverse phonon scattering due to the piezoelectric field [45]

$$|M_{\mathrm{TA-PZ}}(\mathbf{q})|^2 = 2\frac{32\pi^2\hbar(eh_{14})^2}{\epsilon^2\rho c_{\mathrm{TA}}V} \times\left|\frac{q_x^2q_y^2 + q_x^2q_z^2 + q_y^2q_z^2}{|\mathbf{q}|^5} - \frac{(3q_xq_yq_z)^2}{|\mathbf{q}|^7}\right|. \tag{11}$$

Finally, spin relaxation rates are dependent on the transition matrix element $|\langle\psi_0|e^{i\mathbf{q}\cdot\mathbf{r}}|\psi_1\rangle|^2$ which depends on the full three-dimensional confinement. In order to divide the contribution of confinements along the nanowire axis and the yz plane, we write the transition matrix element as $|\langle 0|e^{iq_xx}|1\rangle|^2|T_{yz}|^2$, where $|\langle 0|e^{iq_xx}|1\rangle|^2$ is the contribution along the nanowire direction, while

$$|T_{yz}|^2 = \left|\iint dydz|\Psi(y, z)|^2e^{i(q_yy+q_zz)}\right|^2 \tag{12}$$

represents scattering in a plane perpendicular to the nanowire axis.

The role of $|T_{yz}|^2$ in the spin relaxation rate depends on the regime in which spin qubit operates. At low magnetic fields, when $|\mathbf{q}|z_0 \ll 1$ and $|\mathbf{q}|y_0 \ll 1$, dipole approximation $e^{i\mathbf{q}\cdot\mathbf{r}} \approx 1 + i\mathbf{q}\cdot\mathbf{r}$ is valid [22] and $|T_{yz}|^2$ can be replaced with $(1 + |\mathbf{q}|^2z_0^2\cos^2\theta) \approx 1$, implying that one-dimensional approximation is justified. However, at higher magnetic fields, dipole approximation is not valid and confinement in the yz direction can play a significant role. To determine its role in the spin relaxation rate, we have numerically calculated $|T_{yz}|^2$ beyond the dipole approximation.

Magnetic field strengths for which the system operates outside of the dipole approximation ($|\mathbf{q}|y_0 \geqslant 1$) can be roughly estimated; assuming energy separation between qubit states proportional to $g\mu_BB$, Fermi golden rule determines phonon wave number $|\mathbf{q}| = g\mu_BB/(\hbar c_\lambda)$, where $c_{\mathrm{LA}} = 3800$ m/s [46] and $c_{\mathrm{TA}} = 1900$ m/s [47], giving us magnetic field strengths for the electron-phonon scattering in the longitudinal (0.084 T) and transverse (0.042 T) direction above which we are outside of the dipole approximation.

Before we continue, we provide necessary parameters for the calculation of the spin relaxation rate: $eh_{14} = 1.41 \times 10^9$ eV/m [45], $\epsilon = 16.5$, $D = 7$ eV [48], $\rho = 5775$ kg/m^3 [49].

A. Rabi frequency

We start the discussion of obtained results with the analysis of Rabi frequency dependence on the parameters of interest.

In Fig. 2(a), dependence of Ω_{01} (in eE_0x_0/h units) on $\theta - \varphi$ and magnetic field strength is presented for the QD confinement potential. Our results confirm the expected π periodic behavior with respect to $\theta - \varphi$ [30]. Depending on the magnetic field strength, results can be divided into two classes. In the first class qubit states represent Zeeman sublevels of the orbital ground state; in this regime zero Rabi frequency can be found for special magnetic field orientations ($\theta - \varphi = 0, \pi$), since these qubit states have orthogonal spin components. In the second class, magnetic field strengths have led to rearrangement of energy levels, such that qubit states originate from the ground and the first excited orbital state. In this situation, an orbital qubit is constructed, with a very weak dependence of Ω_{01} on $\theta - \varphi$ ($\Omega_{01} \neq 0$ in the orbital qubit regime for any $\theta - \varphi$). Critical magnetic field value B_c of spin to orbital qubit transition is almost independent on $\theta - \varphi$ and can be easily determined from the eigenspectrum analysis. Alternatively, for $\theta - \varphi = 0, \pi$, abrupt switch of Ω_{01} from zero to the nonzero value at B_c is a fingerprint of the

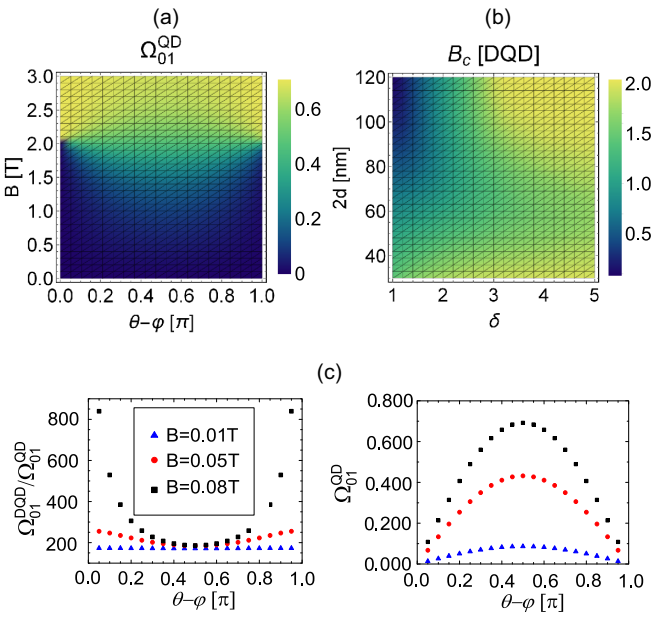

FIG. 2. (a) Dependence of Rabi frequency Ω_{01}^{QD} (in eE_0x_0/h units) on $\theta-\varphi \in (0,\pi)$ and $B \in (0,3)$ T for QD gating potential. (b) In the case of DQD confinement, dependence of B_c on the asymmetry parameter $\delta \in (1,5)$ and distance between the dots $2d \in (30,120)$ nm is given. (c) Dependence of the ratio $\Omega_{01}^{DQD}/\Omega_{01}^{QD}$ on $\theta-\varphi \in (0.05,0.95)\pi$ and magnetic field strengths $B = 0.01$ T, $B = 0.05$ T, and $B = 0.08$ T is presented for the symmetric DQD potential; distance between the dots is equal to $2d = 120$ nm. For the same angle range and magnetic field values Ω_{01}^{QD} in eE_0x_0/h units is presented.

transition. In the case of the QD potential, we extract the critical magnetic field value $B_c \approx 2.04$ T.

Gating with DQD potential gives a qualitatively similar dependence of Ω_{01} on B and $\theta-\varphi$. Being interested in the qualitative comparison of the impacts of QD and DQD potentials, we first establish a basis for comparison between them. To this end, we assume the same frequency of the QD potential and the right dot of the DQD potential, $\omega = \omega_R$, and vary the asymmetry parameter δ and the distance between the dots $2d$. For highly asymmetric DQD confinement and the large interdot distance, the electron will reside on only one dot, i.e., this potential is effectively the same as the single QD potential. The qualitative similarity of the single and double QD potential is checked through the comparison of the probability density of the ground and first excited state (qubit states); similar probability density profiles of the qubit states directly correspond to the similar Rabi frequency values of the two systems. Using the numerical comparison of the probability densities and the Rabi frequency in the case of QD and DQD potential, it can be concluded that for $2d \geqslant 120$ nm and $\delta \geqslant 5$ there is no effective difference between the results arising from two potentials. In other words, one should use $\delta < 5$ and $2d < 120$ nm to test the genuine effects of the DQD potential.

Figure 2(b) depicts the dependence of B_c in the DQD case on $\delta \in (1,5)$ and $2d \in (30,120)$ nm. When compared to the B_c value in the QD case, drastically lower values are found, especially in the case of symmetric confinement with well separated left and right QD. As an example, critical magnetic field value $B_c \approx 0.085$ T for the symmetric DQD confinement with $2d = 120$ nm is roughly 24 times smaller than in the QD case.

Lower B_c for the symmetric DQD confinement is followed by at most factor 3 increase of $\Omega_{01}(B_c^{DQD})$, when compared to $\Omega_{01}(B_c^{QD})$. This slight increase, followed by lower B_c below which symmetric DQD operates, indicates a steeper rise of Rabi frequency for symmetric DQD confinements and the possibility to induce an even bigger difference between Ω_{01}^{DQD} and Ω_{01}^{QD} for the optimal magnetic field configuration. To investigate this possibility, we have performed a numerical analysis of the Rabi frequency ratio $\Omega_{01}^{DQD}/\Omega_{01}^{QD}$ for a wide range of DQD confinements and different magnetic field strengths/orientations, such that both systems operate as spin qubits. Our results confirm that symmetric DQD confinement maximally enhances this ratio when operating at magnetic field strengths close to B_c for the DQD potential, while the field orientation should be chosen such that $\theta-\varphi$ is close to 0 or π. In order to illustrate this conclusion, in the left panel of Fig. 2(c) we present the ratio $\Omega_{01}^{DQD}/\Omega_{01}^{QD}$ for $2d = 120$ nm and $\delta = 1$ in the DQD case, assuming field orientations $\theta-\varphi \in (0.05,0.95)\pi$ and magnetic field strengths $B = 0.01$ T, $B = 0.05$ T, and $B = 0.08$ T ($B_c^{DQD} \approx 0.085$ T for this setup). Since angles $\theta-\varphi = 0,\pi$ should be excluded from the analysis because they correspond to zero Rabi frequency, we have restricted our plots to a $\theta-\varphi$ region smaller than π [see the right panel of Fig. 2(c) for the Ω_{01}^{QD} values], obtaining the highest ratio of around 800. It should be noticed that for angles closer to $0/\pi$ even bigger ratios (10^4) can be obtained, but at the cost of lowering the value of Rabi frequency.

B. Spin relaxation

Another important component for determining spin qubit quality is the spin relaxation rate. Similarly as Rabi frequency, Γ_{01} is dependent on the magnetic field and gating potential. However, Γ_{01} can be additionally dependent on the confinement in yz plane. In order to compare the influence of three-dimensional confinement with the confinement along the nanowire axis solely, we define one-dimensional approximation of the relaxation rate Γ_{01}^{1D} by changing the transition matrix element $|\langle\psi_0|e^{i\mathbf{q}\cdot\mathbf{r}}|\psi_1\rangle|^2$ with $|\langle 0|e^{iq_x x}|1\rangle|^2$ in Eq. (8).

It has been known that in lateral GaAs QDs spin relaxation rates are dominated by piezoelectric field [50,51]. In our case, we wish to analyze the influence of each relaxation channel; thus, the overall spin relaxation rate will be divided into three contributions:

$$\Gamma_{01} = \Gamma_{01}^{LA-DP} + \Gamma_{01}^{LA-PZ} + \Gamma_{01}^{TA-PZ}, \tag{13}$$

each dependent on a different geometric factor, see Eqs. (9)–(11).

Before presenting the numerical results, conclusions independent on the choice of gating potentials are provided. First, Γ_{01} shows oscillatory dependence on the $\theta-\varphi$ angle, being equal to zero for $\theta-\varphi = 0,\pi$ and reaching the maximum for $\theta-\varphi = \pi/2$ in the spin qubit regime [21]. Second, for weak magnetic field strengths ($B < 0.1$ T), piezoelectric fields dominate relaxation rates. At the same time, yz confinement can be ignored.

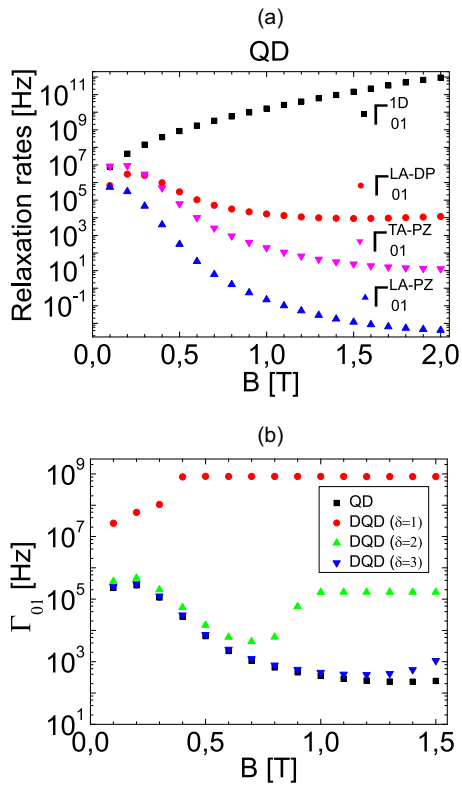

FIG. 3. (a) Dependence of the relaxation rates on the magnetic field strength $B \in (0.1, 2)\,\mathrm{T}$ for $\theta - \varphi = \pi/2$. Red circles represent the contribution of deformation potential in the scattering rates, while inverted pink (blue) triangles show the contribution of piezoelectric field for the electron-phonon scattering in the transverse (longitudinal) direction. Finally, black squares represent relaxation rates in the one-dimensional approximation, in which the contribution of the confinement perpendicular to the nanowire axis is neglected. (b) Dependence of Γ_{01} on the magnetic field strength $B \in (0.1, 1.5)\,\mathrm{T}$ in the case of QD and DQD confinement potential. Magnetic field orientation is chosen such that $\theta - \varphi = 0.05\pi$. In the DQD case, the distance between the dots is set at 90 nm, while the asymmetry parameter is varied.

To explore a new type of behavior accessible in InSb spin qubits, we focus our attention on stronger magnetic fields and investigate its impact on each relaxation channel and one-dimensional approximation of the total relaxation rate Γ_{01}^{1D}. We start from the QD potential. In Fig. 3(a), dependence of relaxation rates on $B \in (0.1, 2)\,\mathrm{T}$ for the fixed angle $\theta - \varphi = \pi/2$ is given [52]. Red circles represent the contribution of deformation potential, pink inverse (blue) triangles denote the impact of piezoelectric field in the electron-phonon scattering along the transverse (longitudinal) direction. Graphs show that relaxation rate Γ_{01}^{LA-PZ} can safely be ignored, while Γ_{01}^{LA-DP} and Γ_{01}^{TA-PZ} have nontrivial influence on Γ_{01}. For weak magnetic fields Γ_{01}^{TA-PZ} term is dominant, while for large magnetic fields Γ_{01}^{LA-DP} should be considered solely [39]. A different influence of Γ_{01}^{TA-PZ} and Γ_{01}^{LA-DP} lies in the opposite behavior of the corresponding geometric factors: $|M_{TA-PZ}(\mathbf{q})|^2$ [$|M_{LA-DP}(\mathbf{q})|^2$] is inversely (directly) proportional to the energy splitting between the Zeeman levels and decreases (increases) with the magnetic field rise.

Contribution of the yz plane confinement on the spin relaxation rate can be determined by comparing the Γ_{01}^{1D} with relaxation rate channels. The comparison is illustrated in Fig. 3(a), clearly demonstrating that one-dimensional approximation of the spin relaxation rate is valid only for weak magnetic fields, below 0.1 T. At higher fields, due to the strong g factor of the InSb material, both $|\mathbf{q}|y_0$ and $|\mathbf{q}|z_0$ are greater than one, triggering the effects of the yz plane confinement for each relaxation rate channel. Thus, suppressed spin relaxation represents a fingerprint of a material with a strong g factor.

In the case of DQD potentials, dependence of B_c on the form of gating presents a serious limitation on the regimes that can be accessed. For example, if the B_c value is sufficiently weak, $B_c < 0.1\,\mathrm{T}$, the spin qubit operates under the dominant influence of the piezoelectric field. A strong magnetic field regime is beneficial for spin qubit operation due to strong Rabi frequency and suppressed spin relaxation. In order to operate in this regime, asymmetric DQD potential should be used. To compare the influence of QD and DQD potential on Γ_{01}, in Fig. 3(b), we plot the dependence of the spin relaxation rate in the case of QD and DQD confinement on the magnetic field strength $B \in (0.1, 1.5)\,\mathrm{T}$, assuming $\theta - \varphi = \pi/2$ and $2d = 90\,\mathrm{nm}$. Besides the symmetric $\delta = 1$ confinement, asymmetric DQD confinements ($\delta = 2, 3$) were analyzed as well. The presented results show that DQD gating leads to increased relaxation rates, when compared to the QD potential. This difference is minimized for highly asymmetric gating potentials. Note that B independent Γ_{01} values suggest that orbital qubit is created: energy difference between the states with the same spin component (representing the orbital qubit states in our case) is independent on B and triggers phonons on the same energy, leading to the observed effect. Consequently, these points should be excluded from the spin qubit analysis.

Finally, we emphasize that in the special case of the asymmetric DQD potential with $\delta = 1.5$ a similar trend of the spin relaxation rate is ascertained [21], i.e., after the increase of the spin relaxation rate in the dominant regime of the piezoelectric field, suppression of spin relaxation is observed, followed by the increase up to magnetic field independent saturation value [see the green triangles in Fig. 3(b) as a comparison].

C. Spin qubit quality

Quantitative estimate of the spin qubit quality can be given with the help of the figure of merit ξ [22],

$$\xi = \frac{\Omega_{01}}{\Gamma_{01} + \Gamma_o}, \tag{14}$$

measuring the number of qubit operations that can be implemented during the qubit lifetime. In Eq. (14) Γ_o represents relaxation rate of decay channels different from phonons. To divide the contribution of phonons from them, we rewrite ξ in terms of the phonon figure of merit $\xi_{ph} = \Omega_{01}/\Gamma_{01}$ and relative influence of other channels with respect to phonons Γ_o/Γ_{01}. Thus,

$$\xi = \frac{\xi_{ph}}{1 + \frac{\Gamma_o}{\Gamma_{01}}}. \tag{15}$$

We first analyze ξ_{ph} for the QD confinement. Neglecting the weak magnetic field regime [53], in Fig. 4 we

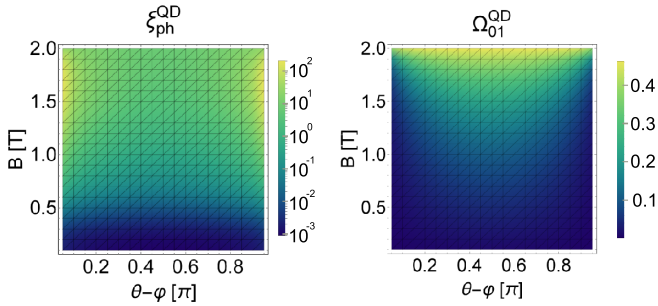

FIG. 4. For the QD confining potential, dependence of the figure of merit $\xi_{\rm ph}^{\rm QD}$ (given in dimensionless unit 7.25 $\frac{\rm m}{\rm V}\times E_0$) and Rabi frequency (in eE_0x_0/h units) on the relative angle $\theta-\varphi\in(0.05, 0.95)\pi$ and magnetic field strength $B\in(0.1, 2)$ T is presented.

present the dependence of $\xi_{\rm ph}^{\rm QD}$ on $B\in(0.1, 2)$ T and $\theta-\varphi\in(0.05, 0.95)\pi$. The restricted $\theta-\varphi$ domain plotted is due to the *a priori* exclusion of $\theta-\varphi=0,\pi$ values ($\Gamma_{01}^{\rm QD}=0$ in these situations). Plots show that to maximal value of $\xi_{\rm ph}^{\rm QD}$ correspond relative angles $\theta-\varphi=0.05\pi, 0.95\pi$. This result suggests that for $\theta-\varphi$ closer to 0 or π than presented even bigger $\xi_{\rm QD}$ values can be obtained, at the cost of lowering the Rabi frequency. In other words, $\Gamma_{01}^{\rm QD}$ has a steeper decline to zero than $\Omega_{01}^{\rm QD}$, when $\theta-\varphi$ goes from $\pi/2$ to 0 or π.

Magnetic field orientation isotropy of $\Gamma_{\rm o}$ [51] implies that shift from $\theta-\varphi=\pi/2$ increases $\Gamma_{\rm o}/\Gamma_{01}^{\rm QD}$ also. Thus, in order to maximize ξ, optimization of both $\xi_{\rm ph}^{\rm QD}$ and $\Gamma_{\rm o}/\Gamma_{01}^{\rm QD}$ is needed. Since at high magnetic fields phonon induced relaxation dominates [51], deviation of $\theta-\varphi$ from $\pi/2$ improves the spin qubit quality until $\Gamma_{\rm o}/\Gamma_{01}^{\rm QD}$ drops below 1. This sets up the optimal magnetic field orientation.

Finally, we compare the impacts of DQD and QD potentials on the spin qubit quality. As discussed in Sec. III A, Rabi frequency in the DQD case can be three orders of magnitude greater than in the QD case. Enhanced Rabi frequency suggests that SOC effects are more pronounced; thus, phonon induced spin relaxation rate should be enhanced. When compared to the QD case, an increase of $\Gamma_{01}^{\rm DQD}$ followed by the negative trend of $\xi_{\rm ph}^{\rm DQD}$ ensures that spin qubit quality decreases; symmetric DQD confinements give the poorest results, while highly asymmetric DQD potentials provide similar values as for QD gating.

IV. CONCLUSIONS

We have investigated the influence of gating potentials, magnetic field strength and orientation on Rabi frequency and spin relaxation rate in a single electron InSb nanowire spin qubit. Due to the strong Landé g factor, we were able to show that InSb spin qubit can operate in the regime in which deformation potential of acoustic phonons dominate relaxation rate. Qualitatively new behavior of spin relaxation rate comes from the confinement perpendicular to the nanowire axis, offering a new regime in which spin qubit can successfully operate. We have shown that gating potential has a crucial role in enabling such a situation, additionally pointing out simple harmonic potential as beneficial for the optimal definition of a spin qubit. Although presented for InSb nanowire spin qubits, conclusions remain valid for spin qubits in other materials with a strong g factor. Thus, modifications of g due to different effects, e.g., strong in-plane magnetic field [54], do not interfere with the conclusions stated in this work.

ACKNOWLEDGMENTS

This research was funded by the Ministry of Education, Science, and Technological Development of the Republic of Serbia under projects ON171035 and ON171027 and the National Scholarship Programme of the Slovak Republic (ID 28226).

APPENDIX A: DERIVATION OF THE EFFECTIVE ONE-DIMENSIONAL HAMILTONIAN

Here we derive the effective one-dimensional Hamiltonian H of the electron in an InSb quantum wire, by averaging the three-dimensional kinetic energy term $T_{\rm 3D}$ and two-dimensional spin-orbit Hamiltonian $H_{\rm so}^{\rm 2D}$ over y and z direction. Thus, we start from the three-dimensional Hamiltonian

$$H_{\rm 3D}=T_{\rm 3D}+V(x)+H_{\rm so}^{\rm 2D}+H_z, \tag{A1}$$

where $T_{\rm 3D}=\sum_{i=x,y,z}P_i^2/2m^*$ ($P_i=p_i+eA_i$),

$$H_{\rm so}^{\rm 2D}=\alpha_R(P_x\sigma_y-P_y\sigma_x)+\alpha_D(P_x\sigma_x-P_y\sigma_y), \tag{A2}$$

while $V(x)$ and H_z are the gating potential and the Zeeman term, defined in Eq. (4) and Eqs. (5) and (6), respectively. The choice of the vector potential components $A_x=-Bz\sin\theta$, $A_y=0$, $A_z=-By\cos\theta$ is such that it corresponds to the applied in-plane magnetic field $\mathbf{B}=B(\cos\theta,\sin\theta,0)$. After averaging the kinetic energy operator over the y and z direction using the ground state wave function $\Psi(y,z)=\psi(y)\psi(z)$, we get

$$\langle T\rangle=\frac{p_x^2}{2m^*}-\frac{eB\langle z\rangle\sin\theta}{m^*}p_x+\left[\frac{\langle p_y^2\rangle}{2m^*}+\frac{\langle(p_z-eBy\cos\theta)^2\rangle}{2m^*}+\frac{e^2B^2\sin^2\theta\langle z^2\rangle}{2m^*}\right]. \tag{A3}$$

In the previous equation, only the first and second term affect the dynamics in the x direction, while all terms in the square brackets can be considered the constant shift of energy and, therefore, can be neglected.

Next, effective one-dimensional spin-orbit interaction Hamiltonian is equal to

$$\begin{aligned}\langle H_{\rm so}\rangle&=\alpha_R((p_x-eB\langle z\rangle\sin\theta)\sigma_y-\langle p_y\rangle\sigma_x)\\&\quad+\alpha_D((p_x-eB\langle z\rangle\sin\theta)\sigma_x-\langle p_y\rangle\sigma_y)\\&=(p_x-eB\langle z\rangle\sin\theta)(\alpha_R\sigma_y+\alpha_D\sigma_x),\end{aligned} \tag{A4}$$

where we have used the fact that expectation value of the momentum p_y, $\langle p_y\rangle=\int_{-\infty}^{\infty}\Psi^*(y,z)p_y\Psi(y,z)$, is explicitly equal to zero.

A further simplification of the effective Hamiltonian can be made by neglecting the term $eB\langle z\rangle\sin\theta\,p_x/m^*$ from Eq. (A3) and $eB\langle z\rangle\sin\theta$ from Eq. (A4). Assuming that intensity of p_x

is proportional to $\hbar/x_0$, magnetic field dependent terms can be neglected if the relation

$$\frac{\hbar}{x_0} \gg eB\langle z\rangle \tag{A5}$$

is satisfied. More concretely, when the $\hbar/x_0$ is for a factor of 10 stronger than the magnetic field dependent term, orbital effects of the magnetic field are small and can be discarded. In our calculations, the magnetic field strengths of interest are up to 3 T, yielding the relation for the z expectation value

$$\langle z\rangle \leqslant 0.1\frac{\hbar}{ex_0 \times 3\ \mathrm{T}} \tag{A6}$$

that has to be satisfied to successfully operate in this regime. As discussed in Sec. II, the wave function $\psi(z)$ is dependent on the strength of the applied electric field E: with the increase of the electric field strength $\langle z\rangle$ increases. In other words, the strength of the electric field is limited from above. Numerical estimate for the critical value of electric field is 6.5×10^6 V/m, going to be used in our numerical calculations. Under these assumptions, the effective one-dimensional Hamiltonian resembles the one defined in Eq. (1), used in the rest of the paper.

APPENDIX B: NUMERICAL SOLUTION OF THE ONE-DIMENSIONAL SCHRÖDINGER EQUATION

In order to find eigenvectors and eigenenergies of the Hamiltonian H, given in Eq. (1), numerical diagonalization is performed. After defining orbital and spin-orbit lengths as x_0 and $x_{so} = \hbar/m\alpha$, respectively, such that $x = x_0 u$, where u is dimensionless variable, H can be written in the following form:

$$H = \frac{\hbar^2}{2m^* x_0^2} H_{\mathrm{red}}. \tag{B1}$$

Eigenvectors of H are the same as of H_{red}, while eigenvalues of H and H_{red} differ for the factor $\hbar^2/2m^* x_0^2$, having the energy units. The benefits of using H_{red} instead of H stems from the transfer into dimensionless units, more suitable for numerical manipulation. The concrete form of H_{red} is equal to

$$H_{\mathrm{red}} = -\frac{d^2}{du^2} - 2i\frac{x_0}{x_{so}}\mathbf{a}\cdot\boldsymbol{\sigma}\frac{d}{du} + V_{\mathrm{eff}}(u) + g_{\mathrm{eff}}\boldsymbol{n}\cdot\boldsymbol{\sigma}, \tag{B2}$$

where g_{eff} and $V_{\mathrm{eff}}(u)$ are effective Landé factor and effective potential, respectively,

$$g_{\mathrm{eff}} = g\frac{m^* x_0^2 \mu_B B}{\hbar^2}, \quad V_{\mathrm{eff}}(u) = \frac{2m^* x_0^2}{\hbar^2} V(x_0 u), \tag{B3}$$

while vectors $\mathbf{a}$ and $\mathbf{n}$ are spin-orbit and magnetic field unit vectors, respectively, defined in the main text. The form of effective potential depends on the choice of gating potential (5) and (6), while effective Landé factor is linearly dependent on the magnetic field strength B.

To numerically solve the eigenproblem of H_{red}, orbital space is discretized with an uniform grid. First and second derivative of a wave function are approximated by finite difference uniform grid formulas [55]

$$\frac{d\psi(u)}{du} = \frac{\psi_{-4}}{280h} - \frac{4\psi_{-3}}{105h} + \frac{\psi_{-2}}{5h} - \frac{4\psi_{-1}}{5h} - \frac{\psi_4}{280h} + \frac{4\psi_3}{105h} - \frac{\psi_2}{5h} + \frac{4\psi_1}{5h} + O(h^8), \tag{B4}$$

$$\frac{d^2\psi(u)}{du^2} = -\frac{\psi_{-4}}{560h^2} + \frac{8\psi_{-3}}{315h^2} - \frac{\psi_{-2}}{5h^2} + \frac{8\psi_{-1}}{5h^2} - \frac{205\psi_0}{72h^2} - \frac{\psi_4}{560h^2} + \frac{8\psi_3}{315h^2} - \frac{\psi_2}{5h^2} + \frac{8\psi_1}{5h^2} + O(h^8), \tag{B5}$$

with accuracy to the h^8 order, where h is the uniform grid step. By definition, $\psi_{\pm n} = \psi(u \pm nh)$ represent wave functions shifted in the left/right $(-/+)$ direction of the coordinate space for nh.

Uniform grid formulas allow us to represent the Hamiltonian as a square matrix. Effective potential is represented as a diagonal matrix, while matrix representation of the first and second order derivative have nondiagonal terms in addition. Since H_{red} is dependent on spin degrees of freedom also, the orbital part of the Hamiltonian is trivially extended in the spin space. Also, the Zeeman Hamiltonian is trivially extended in the orbital space, while the matrix form of the spin-orbit Hamiltonian is obtained as a tensor product of the first derivative matrix and spin Hamiltonian $\mathbf{a}\cdot\boldsymbol{\sigma}$.

In the QD case, harmonic potential is centered at $u = 0$, while in the case of DQD potential numerical calculations assumed each QD center range from $u = \pm 1/2$ to $u = \pm 2$. We have checked that for all studied situations the choice of u from the interval $(-8, 8)$ is enough to capture the smooth decline of the orbital wave function to 0 at $u = \pm 8$. Also, the division of the orbital space into $N = 2000$ parts was enough to ensure convergence of the results, i.e., for the increase of N to 4000 the relative difference between the results is below 10^{-4}.

[1] C. H. Bennett and D. P. DiVincenzo, Nature (London) **404**, 247 (2000).

[2] F. H. L. Koppens, C. Buizert, K. J. Tielrooij, I. T. Vink, K. C. Nowack, T. Meunier, L. P. Kouwenhoven, and L. M. K. Vandersypen, Nature (London) **442**, 766 (2006).

[3] D. Press, T. D. Ladd, B. Zhang, and Y. Yamamoto, Nature (London) **456**, 218 (2008).

[4] V. N. Golovach, M. Borhani, and D. Loss, Phys. Rev. B **74**, 165319 (2006).

[5] K. C. Nowack, F. H. L. Koppens, Yu. V. Nazarov and L. M. K. Vandersypen, Science **318**, 1430 (2007).

[6] R. Brunner, Y.-S. Shin, T. Obata, M. Pioro-Ladriére, T. Kubo, K. Yoshida, T. Taniyama, Y. Tokura, and S. Tarucha, Phys. Rev. Lett. **107**, 146801 (2011).

[7] E. Kawakami, P. Scarlino, D. R. Ward, F. R. Braakman, D. E. Savage, M. G. Lagally, M. Friesen, S. N. Coppersmith, M. A. Eriksson, and L. M. K. Vandersypen, Nat, Nanotechnol. **9**, 666 (2014).

[8] K. Takeda, J. Yoneda, T. Otsuka, T. Nakajima, M. R. Delbecq, G. Allison, Y. Hoshi, N. Usami, K. M. Itoh, S. Oda, T. Kodera, and S. Tarucha, npj Quantum Inf. **4**, 54 (2018).

[9] D. V. Khomitsky, L. V. Gulyaev, and E. Ya. Sherman, Phys. Rev. B **85**, 125312 (2012).

[10] D. V. Khomitsky, E. A. Lavrukhina, and E. Ya. Sherman, Phys. Rev. B **99**, 014308 (2019).

[11] A. V. Khaetskii and Y. V. Nazarov, Phys. Rev. B **61**, 12639 (2000).

[12] A. V. Khaetskii and Y. V. Nazarov, Phys. Rev. B **64**, 125316 (2001).

[13] D. Mozyrsky, S. Kogan, V. N. Gorshkov, and G. P. Berman, Phys. Rev. B **65**, 245213 (2002).

[14] C. Tahan, M. Friesen, and R. Joynt, Phys. Rev. B **66**, 035314 (2002).

[15] E. Ya. Sherman and D. J. Lockwood, Phys. Rev. B **72**, 125340 (2005).

[16] P. Stano and J. Fabian, Phys. Rev. B. **72**, 155410 (2005).

[17] F. Baruffa, P. Stano, and J. Fabian, Phys. Rev. Lett. **104**, 126401 (2010).

[18] X. Linpeng, T. Karin, M. V. Durnev, R. Barbour, M. M. Glazov, E. Ya. Sherman, S. P. Watkins, S. Seto, and K.-M. C. Fu, Phys. Rev. B **94**, 125401 (2016).

[19] V. N. Stavrou, J. Phys.: Condens. Matter **29**, 485301 (2017).

[20] V. N. Stavrou, J. Phys.: Condens. Matter **30**, 455301 (2018).

[21] Z.-H. Liu, R. Li, X. Hu, and J. Q. You, Sci. Rep. **8**, 2302 (2018).

[22] O. Malkoc, P. Stano, and D. Loss, Phys. Rev. B **93**, 235413 (2016).

[23] J. I. Climente, A. Bertoni, G. Goldoni, M. Rontani, and E. Molinari, Phys. Rev. B **75**, 081303(R) (2007).

[24] D. Chaney and P. A. Maksym, Phys. Rev. B **75**, 035323 (2007).

[25] E. Reyes-Gómez, N. Porras-Montenegro, C. A. Perdomo-Leiva, H. S. Brandi, and L. E. Oliveira, J. Appl. Phys. **104**, 023704 (2008).

[26] H. A. Nilsson, P. Caroff, C. Thelander, M. Larsson, J. B. Wagner, L.-E. Wernersson, L. Samuelson, and H. Q. Xu, Nano Lett. **9**, 3151 (2009).

[27] M. Trif, V. N. Golovach, and D. Loss, Phys. Rev. B **77**, 045434 (2008).

[28] S. Nadj-Perge, S. M. Frolov, E. P. A. M. Bakkers, and L. P. Kouwenhoven, Nature (London) **468**, 1084 (2010).

[29] S. Nadj-Perge, V. S. Pribiag, J. W. G. van den Berg, K. Zuo, S. R. Plissard, E. P. A. M. Bakkers, S. M. Frolov, and L. P. Kouwenhoven, Phys. Rev. Lett. **108**, 166801 (2012).

[30] R. Li, J. Q. You, C. P. Sun, and F. Nori, Phys. Rev. Lett. **111**, 086805 (2013).

[31] R. Li and J. Q. You, Phys. Rev. B **90**, 035303 (2014).

[32] G. Dresselhaus, Phys. Rev. **100**, 580 (1955).

[33] E. I. Rashba, Fiz. Tv. Tela (Leningrad) **2**, 1224 (1960); Sov. Phys. Solid State **2**, 1109 (1960).

[34] M. Raith, P. Stano, and J. Fabian, Phys. Rev. B **83**, 195318 (2011).

[35] M. Raith, P. Stano, and J. Fabian, Phys. Rev. B **86**, 205321 (2012).

[36] S. Wu, L. Cheng, H. Yu, and Q. Wang, Phys. Lett. A **382**, 1922 (2018).

[37] F. N. M. Froning, M. K. Rehmann, J. Ridderbos, M. Brauns, F. A. Zwanenburg, A. Li, E. P. A. M. Bakkers, D. M. Zumbühl, and F. R. Braakman, Appl. Phys. Lett. **113**, 073102 (2018).

[38] D. Fan, S. Li, N. Kang, P. Caroff, L. B. Wang, Y. Q. Huang, M. T. Deng, C. L. Yu, and H. Q. Xu, Nanoscale **7**, 14822 (2015).

[39] M. P. Nowak and B. Szafran, Phys. Rev. B **89**, 205412 (2014).

[40] Z.-H. Liu, O. Entin-Wohlman, A. Aharony, and J. Q. You, Phys. Rev. B **98**, 241303(R) (2018).

[41] M. Cardona, N. E. Christensen, and G. Fasol, Phys. Rev. B **38**, 1806 (1988).

[42] H. A. Nilsson, O. Karlström, M. Larsson, P. Caroff, J. N. Pedersen, L. Samuelson, A. Wacker, L. E. Wernersson, and H. Q. Xu, Phys. Rev. Lett. **104**, 186804 (2010).

[43] Z.-H. Liu and R. Li, AIP Adv. **8**, 075115 (2018).

[44] R. de Sousa and S. Das Sarma, Phys. Rev. B **68**, 155330 (2003).

[45] J. I. Climente, A. Bertoni, G. Goldoni, and E. Molinari, Phys. Rev. B **74**, 035313 (2006).

[46] S. E. Hebboul and J. P. Wolfe, Phys. Rev. B **34**, 3948 (1986).

[47] O. Madelung, Ed., *Intrinsic Properties of Group IV Elements and III-V, II-VI and I-VII Compounds*, Landolt-Bornstein, New Series Vol. 22 (Springer, Berlin, 1987), Chap. 2.15, p. 130.

[48] C. F. Destefani and S. E. Ulloa, Phys. Rev. B **72**, 115326 (2005).

[49] I. M. Tsidilkovskii and K. M. Demchuk, Phys. Status Solidi B **44**, 293 (1971); K. M. Demchuk and I. M. Tsidilkovskii, *ibid.* **82**, 59 (1977); K. Tukioka, Jpn. J. Appl. Phys. **30**, 212 (1991).

[50] J. L. Cheng, M. W. Wu, and C. Lü, Phys. Rev. B **69**, 115318 (2004).

[51] L. C. Camenzind, L. Yu, P. Stano, J. D. Zimmerman, A. C. Gossard, D. Loss, and D. M. Zumbühl, Nat. Commun. **9**, 3454 (2018).

[52] Although dependence of relaxation rates on the magnetic field strength are presented for the special $\theta - \varphi = \pi/2$ magnetic field orientation, conclusion remain valid for different $\theta - \varphi$ angles.

[53] Low fields correspond to weak Zeeman splitting. In this case low temperatures are needed, such that Zeeman splitting is above the thermal broadening; temperature dependence analysis is beyond the scope of the presented work.

[54] P. Stano, C.-H. Hsu, M. Serina, L. C. Camenzind, D. M. Zumbühl, and D. Loss, Phys. Rev. B **98**, 195314 (2018).

[55] B. Fornberg, Math. Comput. **51**, 699 (1988).

BPU11 CONGRESS

28 August 2022 - 1 September 2022

Book of Abstracts

Editors: Antun Balaž, Goran Djordjević,
Jugoslav Karamarković, Nenad Lazarević

Belgrade, 2022

3. A.G. Petrov et al., JOAM 9, 420 (2007).
4 G.B. Hadjichristov et al., J. Appl. Phys. 115, 083107 (2014).

S06-CMPSP-217 / **Poster presentation**

Mobility of Holstein polaron from real and imaginary time quantum Monte Carlo calculations

Authors: Nenad Vukmirovic[1]; Suzana Miladic[1]

[1] *Institute of Physics Belgrade, University of Belgrade, Serbia*

Presenter: S. Miladic (suzana@ipb.ac.rs)

Electron-phonon (e-ph) interaction is responsible for majority of transport phenomena in condensed matter. In this work, we consider the short-range (localized) e-ph interaction described by the Holstein Hamiltonian. We develop numerically exact path integral Monte Carlo (PIMC) methods to obtain current-current correlation functions (CFs) and polaron mobility of one-dimensional Holstein model.

Generally, several challenges need to be overcome to reliably calculate dynamical properties using the PIMC methods. First one is the dynamical sign-problem of real time CFs which can be eliminated by doing calculations in imaginary time and then analytically continuing to real time. The other challenge is that there is not a reliable method for analytic continuation of numerically obtained values. We overcome these limitations by combining real time and imaginary time calculations with singular value decomposition method for analytical continuation.

For weaker e-ph interaction strengths we were able to calculate CFs in real time for a range of temperatures by using a Monte Carlo algorithm derived from momentum representation of electronic degrees of freedom and coordinate representation of phonons. For stronger interactions such an algorithm leads to a significant sign-problem for longer times and better results are obtained by using a different algorithm. This algorithm is derived from site representation of electronic degrees of freedom and coordinate representation of phonons. The phonon coordinates are then integrated out analytically and Monte Carlo summation over electronic states is performed. In the case of stronger interactions, where real time calculations cannot be used to obtain CFs at longer times, doing analytic continuation of both real time and imaginary time data gives much better results. The methods described enabled us to calculate polaron mobility for a range of temperatures and e-ph interaction strengths.